

1 Characterization of urban amine-containing particles in Southwestern China: seasonal  
2 variation, source, and processing

3 Yang Chen<sup>1,2\*</sup>, Mi Tian<sup>1</sup>, Rujin Huang<sup>2</sup>, Guangming Shi<sup>4</sup>, Huanbo Wang<sup>1</sup>, Chao Peng<sup>1</sup>,  
4 Junji Cao<sup>2</sup>, Qiyuan Wang<sup>2</sup>, Shumin Zhang<sup>3</sup>, Dongmei Guo<sup>3</sup>, Leiming Zhang<sup>5</sup>, and  
5 Fumo Yang<sup>1,4,\*</sup>

6 <sup>1</sup>Research Center for Atmospheric Environment, Chongqing Institute of Green and  
7 Intelligent Technology, Chinese Academy of Sciences, Chongqing 400714, China.

8 <sup>2</sup>Key Lab of Aerosol Chemistry & Physics, State Key Laboratory of Loess and  
9 Quaternary Geology, Institute of Earth Environment, Chinese Academy of Sciences,  
10 Xi'an 710061, China.

11 <sup>3</sup>School of Basic Medical Sciences, North Sichuan Medical College, Nanchong 637000,  
12 Sichuan, China.

13 <sup>4</sup>College of Architecture and Environment, Sichuan University, Chengdu 610065,  
14 China

15 <sup>5</sup>Air Quality Research Division, Science and Technology Branch, Environment and  
16 Climate Change Canada, Toronto M3H 5T4, Canada

17 Correspondence to: Yang Chen (chenyang@cigit.ac.cn); Fumo Yang  
18 (fmyang@cigit.ac.cn)

19 Keyword: single particle; amine; urban environment, processing

20

21

## **Abstract**

22 Amine-containing particles were characterized in an urban area of Chongqing during  
23 both summer and winter using a single particle aerosol mass spectrometer (SPAMS).  
24 Among the collected particles, 12.7% were amine-containing in winter and 8.3% in  
25 summer. Amines were internally mixed with elemental carbon (EC), organic carbon  
26 (OC), sulfate, and nitrate. Diethylamine (DEA) was the most abundant among amine-  
27 containing particles. Wintertime amine-containing particles were mainly from the  
28 northwest direction where a forest park was located; in summer, they were from the  
29 northwest and southwest (traffic hub) directions. These origins suggest that vegetation  
30 and traffic were the primary sources of particulate amines. The average relative peak  
31 area of DEA depended strongly on humidity, indicating that the enhancement of DEA  
32 was possibly due to increasing aerosol water content and aerosol acidity. Using an  
33 adaptive resonance theory neural network (ART-2a) algorithm, four major types of  
34 amine-containing particles were clustered including amine-organic-carbon (A-OC), A-  
35 OCEC, DEA-OC, and A-OCEC-aged. The identified particle types implied that amines  
36 were undergone uptake by particles produced from traffic and biomass burning.  
37 Knowledge gained in this study is useful to understand the atmospheric processing,  
38 origin, and sources of amine-containing particles in the urban area of Chongqing.

39

## 40        **1. Introduction**

41    Amines are ubiquitous in the atmosphere and have both natural (ocean, biomass burning,  
42    and vegetation) and anthropogenic (animal husbandry, industry, combustion, and traffic)  
43    emission sources (Ge et al., 2011a). Trimethylamine (TMA) is one of the most abundant  
44    amines with an estimated global emission flux of 170Gg year<sup>-1</sup> (Ge et al., 2011a).  
45    Gaseous amines compete with ammonia in acid-base reactions, participate in gas-  
46    particle partitioning, and contribute to wet and dry deposition (Angelino et al., 2001;  
47    Monks, 2005; Gómez Alvarez et al., 2007; De Haan et al., 2011; Huang et al., 2012;  
48    You et al., 2014). Gaseous amines also play an essential role in new particle formation  
49    via enhancing the ternary nucleation of H<sub>2</sub>SO<sub>4</sub>-H<sub>2</sub>O clusters in remote areas (Bzdek et  
50    al., 2012; Kirkby et al., 2011). In polluted areas, H<sub>2</sub>SO<sub>4</sub>-diethylamine (DMA)-water  
51    clusters were important during the new particle formation events (Yao et al., 2018).  
52    Amines are also essential in the growth of ambient particles. For example, particulate  
53    aminium salts, which were produced via amine-acid neutralization, tended to prevent  
54    the coagulation between pre-existing particles leading to increased particle number  
55    concentrations (Wang et al., 2010; Smith et al., 2010). Moreover, the enrichment of  
56    TMA had been observed in cloud and fog processing (Zhang et al., 2012; Rehbein et  
57    al., 2011). Characterization of amine-containing particles is important to evaluate their  
58    processing and impact.

59    Single particle mass spectrometers (SPMS), such as aerosol time-of-flight mass  
60    spectrometer (ATOFMS) and Single Particle Aerosol Mass Spectrometer (SPAMS),  
61    have been widely used in real-time measurements of amine-containing particles for  
62    chemical composition and mixing state (Li et al., 2017). SPAMS is different from the  
63    Aerodyne soot-particle aerosol mass spectrometer (SP-AMS), which is a type of aerosol

64 mass spectrometer (AMS) for detecting black carbon, sulfate, nitrate, ammonium,  
65 chloride, and organics (Onasch et al., 2012; Wang et al., 2016). The chemical  
66 composition and mixing state of TMA-containing particles have been reported  
67 worldwide, such as in California, USA (Denkenberger et al., 2007; Qin et al., 2012));  
68 Ontario, Canada (Tan et al., 2002; Rehbein et al., 2011); Mexico City (Moffet et al.,  
69 2008)); European cities (Barcelona, Cork, Zurich, Paris, Dunkirk and Corsica (Healy  
70 et al., 2015; Dall'Osto et al., 2016)), and Chinese cities such as Guangzhou, Shanghai  
71 and Xi'an (Zhang et al., 2012; Chen et al., 2016; Huang et al., 2012). Characterization  
72 of amine-containing particles varied in these locations. In the five European cities such  
73 as Cork, Paris, Dunkirk, Corsica, and Zurich, amines were found internally mixed with  
74 sulfate and nitrate; but in Corsica, amines were internally mixed with methanesulfonate  
75 (Healy et al., 2015). In Barcelona, five unique types of amine-containing particles were  
76 observed (Dall'Osto et al., 2016). In a rural area site in the Pearl River Delta (China),  
77 the marker ion,  $(C_2H_5)_2NH_2^+$ , was the most abundant (90% and 86% of amine-  
78 containing particles in summer and winter)(Cheng et al., 2018). In Guangzhou, TMA-  
79 containing particles were important (Zhang et al., 2012). In previous studies, reported  
80 high RH conditions and fog processing were favorable for the enhancement of  
81 trimethylamine in the particle phase. Zhang et al. (2012) reported a similar scenario in  
82 Guangzhou, China. Thus the location-specific studies in the varied environments are  
83 still necessary.

84 The knowledge of amine-containing particles is limited in southwestern China. In this  
85 region, Chongqing is a megacity with a population of 8.23 million. The city is  
86 subtropical, industrial, and polluted (Chen et al., 2017; Tao et al., 2017). Fog events  
87 frequently occurred in this area, and hence, it is known as the “fog city” in China. The  
88 effect of high relative humidity (RH) on the processing of amine-containing particles

89 needs investigation. This study aims to characterize the amine-containing particles,  
90 including chemical composition, mixing state, atmospheric processing, and source in  
91 Chongqing during winter and summer.

## 92 **2. Methods**

### 93 **2.1 Sampling site**

94 Ambient single particles were collected at an urban air quality supersite from  
95 07/05/2016 to 08/14/2016 (referred to as a summer season) and from 01/21/2016 to  
96 02/25/2016 (referred to as a winter season). The supersite has been described in our  
97 previous studies (Chen et al., 2017). Briefly, the supersite is located on the rooftop of a  
98 commercial office building (106.51°E, 29.62°N) at a height of 30 m above the ground  
99 (Figure S1). The building is surrounded by business and residential communities and is  
100 15 km from the city center. A 3 km<sup>2</sup> forest park is located northwest of the sampling  
101 site and a traffic hub in the southwest.

### 102 **2.2 Instrumentation**

103 A SPAMS (Hexin Inc. Guangzhou, China, model 0515) was deployed for single  
104 particle sampling, and the technical description of SPAMS is available in the literature  
105 (Li et al., 2011; Chen et al., 2017). Briefly, after passing through a diffusive dryer,  
106 particles in a size range of 0.1–2.0 μm are sampled via an aerodynamic lens and form  
107 a particle beam. Particles in the beam come across two pre-positioned laser beams (Nd:  
108 YAG, 532 nm) one-by-one, and the vacuum aerodynamic diameter ( $D_{va}$ ) of each  
109 particle is determined via its time-of-flight. Particles are ionized using an Nd: YAG  
110 laser operating at a wavelength of 266 nm. The yielded ions are analyzed using a bipolar

111 time-of-flight mass spectrometer. Due to the limitation of SPAMS, quantification of  
112 particulate amines was not attempted.

### 113 **2.3 Data analysis**

114 The SPAMS data were imported into the YAADA toolkit (Software Toolkit to Analyze  
115 Single-Particle Mass Spectral Data, v 2.11) to form a single particle dataset. The  
116 analysis was conducted using the marker ions of amines.:  $m/z$  59  $[(\text{CH}_3)_3\text{N}]^+$  (TMA),  
117 74  $[(\text{C}_2\text{H}_5)_2\text{NH}_2]^+$  (diethylamine, DEA), 86  $[(\text{C}_2\text{H}_5)_2\text{NCH}_2]^+$  or  $[\text{C}_3\text{H}_7\text{NHC}_2\text{H}_4]^+$  (DEA  
118 or DPA), 101  $[(\text{C}_2\text{H}_5)_3\text{N}]^+$  (TEA), 102  $[(\text{C}_3\text{H}_7)_2\text{NH}_2]^+$  (DPA), 114  $[(\text{C}_3\text{H}_7)_2\text{NCH}_2]^+$   
119 (DPA), and 143  $[(\text{C}_3\text{H}_7)_3\text{N}]^+$ (TPA) (Healy et al., 2015). Firstly,  $m/z$  59 was used for  
120 querying the TMA-containing particles;  $m/z$  74 for the DEA-containing particles and  
121  $m/z$  86 for TEA-containing particles, and so on. *After the duplicate particles were  
122 removed from the query results, all amine-containing particles were combined into an  
123 amine-containing particle cluster.* Various amines could be both internally and  
124 externally mixed in these particle clusters.

125 An adaptive resonance theory based neural network algorithm (ART-2a) was applied  
126 to cluster the amine-containing particle types using a vigilance factor of 0.70, a learning  
127 rate of 0.05, and 20 iterations (Song et al., 1999). This procedure produced 67 clusters  
128 in summer and 75 clusters in winter; many of these clusters exhibited identical mass  
129 spectra with slight differences in specific ion intensities. A well-established combining  
130 strategy, on the basis of similar mass spectra, temporal trends, and size distribution, was  
131 adopted to merge these particle clusters into the finalized particle types (Dallosto and  
132 Harrison, 2006). *In addition, the relative peak area (RPA) is defined as the peak area of  
133 each  $m/z$  divided by the total dual-ion mass spectral peak areas of each particle (Healy*

134 et al., 2013). The RPA of DEA among the particle type was first calculated from each  
135 DEA-containing particle, and then summed up for detailed analysis.

### 136 **3. Results and discussion**

#### 137 **3.1 Single particle chemical composition and seasonal variation**

138 The percentage of amine-containing particles was 12.7% in the winter SPAMS dataset  
139 and 8.3% in the summer dataset. The DEA-containing particles were dominant,  
140 accounting for 70% and 78% in winter and summer, respectively, while TMA-  
141 containing particles were minor, accounting for up to 7% in winter and 3% in summer.  
142 The average mass spectra of DEA-, DPA, and TMA-containing particles are provided  
143 in Figure S2, and these spectra showed strong homogeneity. The determination  
144 coefficient ( $R^2$ ) between DEA- and DPA- containing particles was 0.98, and  $R^2$  between  
145 DEA- and TMA- containing particles was 0.83.

146 Figure 1 shows the digital mass spectra of amine-containing particles in two seasons.  
147 In each spectrum, the ion height indicates its mixing fraction in the amine-containing  
148 particle dataset, and the stacked color map shows the corresponding ion intensity ranges.  
149 The assignment of ions is shown in Table S1. In both seasons, the dominant ions were  
150  $K^+$  ( $m/z$  39 and 41), amines ( $m/z$  59, 74, and 86), and organics ( $m/z$  43, 51, 63, and 77).  
151 The mixing ratios of ammonium ( $NH_4^+$ ,  $m/z$  18) and polycyclic aromatic hydrocarbons  
152 (e.g.,  $m/z$  116 ( $[C_9H_8]^+$ ), 129 ( $[C_{10}H_9]^+$ ), 140 ( $[C_{11}H_8]^+$ ), and 153 ( $[C_{12}H_9]^+$ )) were  
153 higher in winter than in summer. The strong signal of  $NH_4^+$  was possibly due to the  
154 lower temperature (8°C) in winter than in summer (31°C). The mixing ratios of  $m/z$  59  
155 were 45% and 44% during summer and winter, respectively.

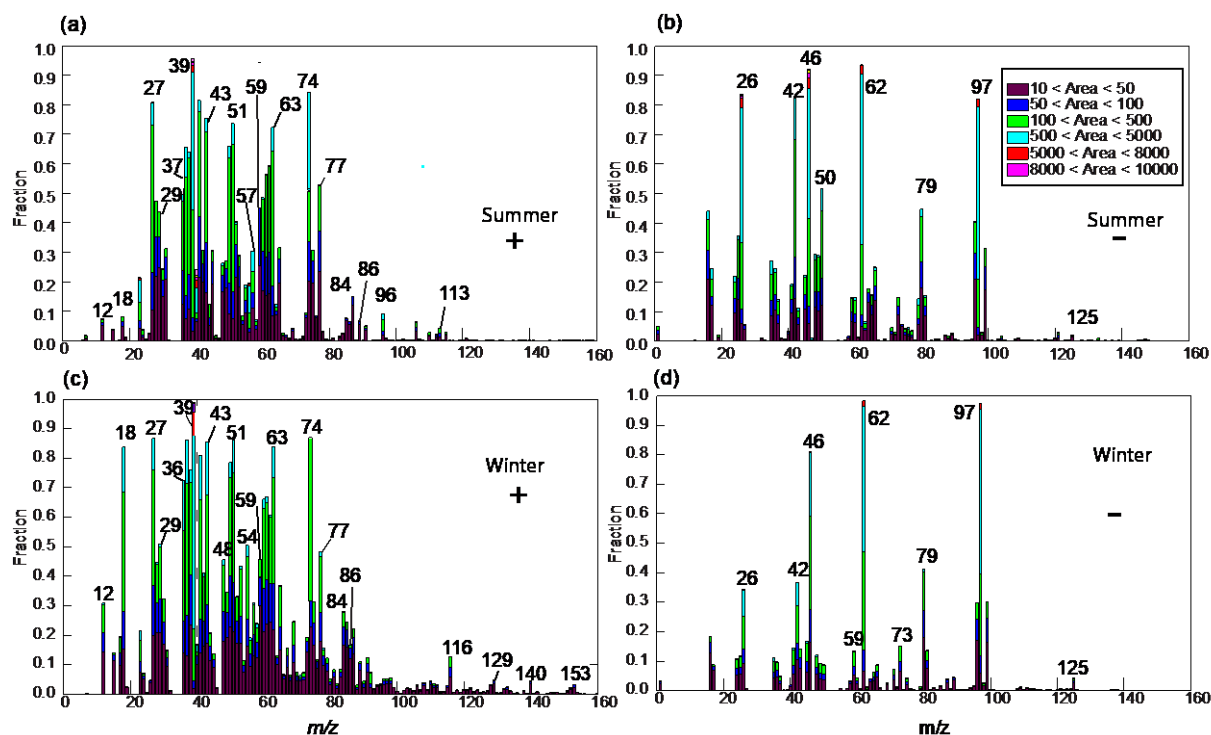
156 In the negative mass spectra of two seasons (Figures 1(b) and 1(d)), the dominant ions  
157 were  $\text{CN}^-$  ( $m/z$  -26),  $\text{CNO}^-$  ( $m/z$  -42), nitrate ( $m/z$  -46 and -62), phosphate (-79), and  
158 sulfate ( $m/z$  -80 and -97). Primary species, such as  $\text{CN}^-$  and  $\text{CNO}^-$  were commonly  
159 from biomass burning (BB) and organonitrogen (Pratt et al., 2011). Levoglucosan  
160 markers from BB, such as -45, -59, and -71 were also detected. Dust markers, such as  
161  $[\text{SiO}_2]^-$  ( $m/z$  -60),  $[\text{}^{28}\text{SiO}_3]^-$  or  $[\text{AlO}_2(\text{OH})]^-$  (-76), and  $[\text{PO}_3]^-$ , were also detected during  
162 summertime, suggesting the influence of dust particles.

163 Seasonal variations of chemical composition and unscaled size distribution are  
164 available in supporting information. Prior to comparison, the ion peak was normalized  
165 using the method developed by Qin et al. (2012). Briefly, the peak area of each  $m/z$  was  
166 divided by the total mass spectral peak area matrix. The normalized ion intensity of the  
167 wintertime particles was subtracted from that of the summertime particles. A positive  
168 value indicates the normalized ion intensity was greater in the summer, whereas a  
169 negative value indicates that the normalized ion intensity was greater in the winter. As  
170 shown in Figure S3,  $\text{Ca}^+$  ( $m/z$  40) and  $\text{Fe}^+$  ( $m/z$  56) were more prevalent during summer.  
171 Organic species, such as  $\text{C}_2\text{H}_3^+$  ( $m/z$  27),  $\text{C}_4\text{H}_3^+$  ( $m/z$  51),  $\text{C}_5\text{H}_3^+$  ( $m/z$  63), and  $\text{C}_6\text{H}_5^+$   
172 ( $m/z$  77) typically from aromatic hydrocarbons, were also more abundant in summer.  
173 During wintertime, signals of sulfate ( $m/z$  -97),  $\text{NO}_3^-$  ( $m/z$  -62),  $\text{NH}_4^+$  ( $m/z$  18), and  $\text{K}^+$   
174 ( $m/z$  39) were more prominent than in summer, suggesting that the wintertime particles  
175 contained more secondary species than those in summer.

176 The unscaled size distribution of amine-containing particles also showed strong  
177 seasonal variations (Figure S4). Generally, amine-containing particles had monomodal  
178 size distributions in the droplet mode; and the distributions peaked at a larger  $D_{\text{va}}$  in  
179 summer than winter. For example, DEA-containing particles peaked at 0.6  $\mu\text{m}$  in winter



180 and 0.8  $\mu\text{m}$  in summer, and DPA-containing particles at 0.7  $\mu\text{m}$  in winter and 0.9  $\mu\text{m}$   
 181 in summer. The size distributions of the major amine-containing particles suggested  
 182 that these particles had undergone substantial aging processes.



183

184 Figure 1. (a) and (c): the positive digital mass spectrum of amine-containing particles  
 185 during summer and wintertime, respectively; (b) and (d): the negative digital mass  
 186 spectrum during summer and wintertime, respectively. The ion height indicates its  
 187 fraction in the amine-containing particle dataset, and the stacked color map indicates  
 188 the ion peak area range.

### 189 3.2 Temporal trend, diurnal pattern, and origin of amine-containing particles

190 Figure 2 shows the temporal trends of RH, temperature, number count, and the peak area  
 191 of amine-containing particles. The winter temperature was lower ( $8.0 \pm 4.0^\circ\text{C}$ ) than  
 192 summer ( $31 \pm 4^\circ\text{C}$ ), and RH in the winter was slightly higher ( $70 \pm 14\%$  versus  $64 \pm 16\%$ )  
 193 (Table 2). Stagnant air conditions occurred in both seasons due to the low wind speeds

194 (Huang et al., 2017), and the winter wind speed was lower than in summer. The hourly  
 195 count of amine-containing particles was typically ten times higher in winter than  
 196 summer.

197 In winter, a good correlation existed between the temporal trends of hourly number  
 198 count and peak area of DEA-containing particles ( $R^2 = 0.86$ ). The corresponding  $R^2$  in  
 199 wintertime DPA-containing particles was 0.88. No such correlation for TMA-  
 200 containing particles was observed in winter ( $R^2 = 0.22$ ) or summer (Figure 2). The  
 201 hourly counts of DEA- and DPA-containing particles were well correlated in both  
 202 summer ( $R^2 = 0.63$ ) and winter ( $R^2 = 0.87$ ), but a weak correlation ( $R^2 = 0.25$ ) existed  
 203 between DEA- and TMA-containing particles. These results suggest DEA- and DPA-  
 204 containing particles were possibly from the same sources.

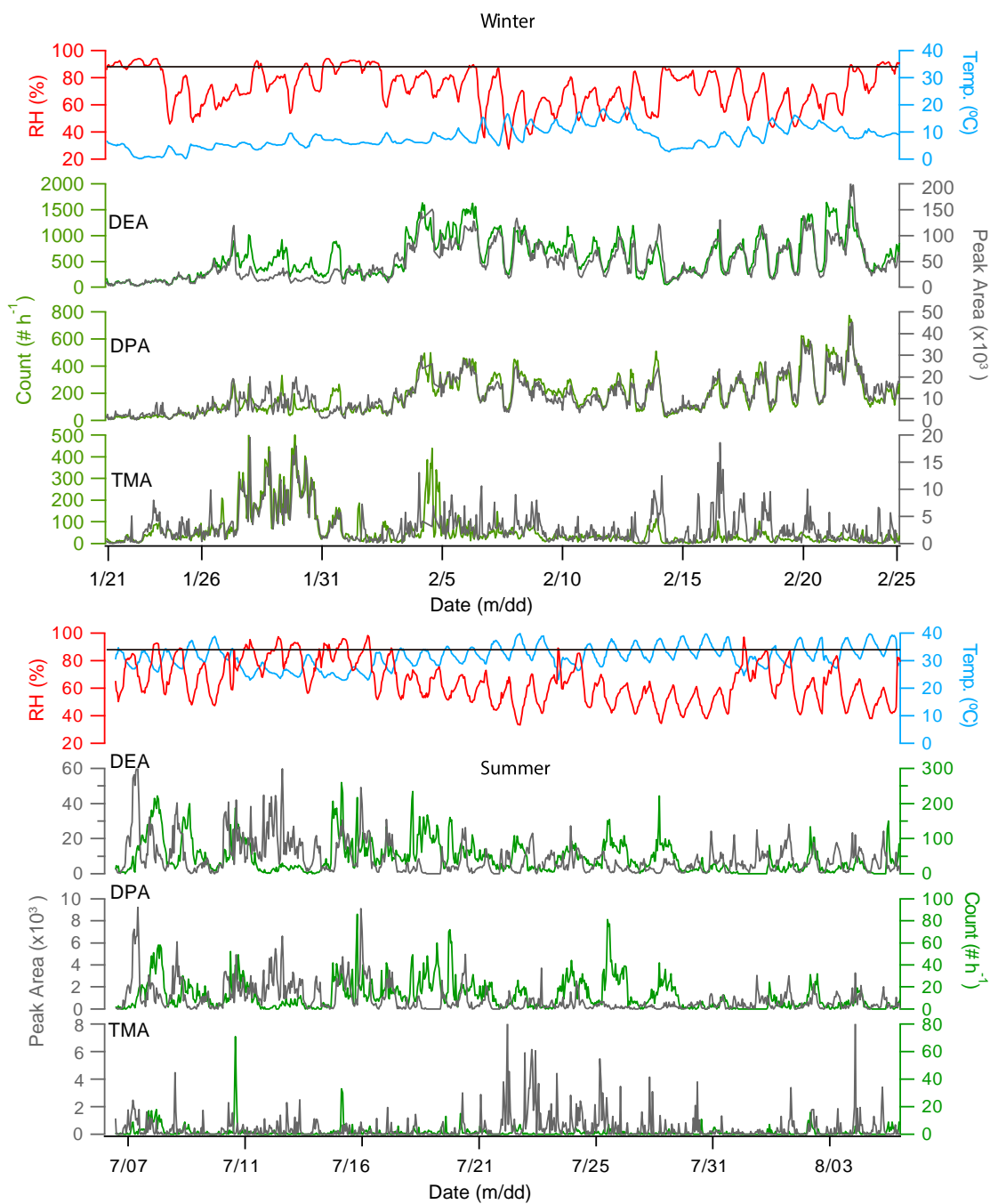
205 Table 2. Meteorological factors and particle counts in summer and winter.

	Winter	Summer
206 Temperature (°C)	8 ±4	31±4
207 Relative humidity (%)	70±14	64±16
208 Wind Speed	1.2±0.7	1.5±1.0
209 <a href="#">Amine</a> -particle Count (# h <sup>-1</sup> )	587±384	47±26

210 DEA- and DPA-containing particles remained at low levels from 1/20/2016 to  
 211 01/26/2016 and averaged at 109 and 26 count h<sup>-1</sup>, respectively. During this period, wind  
 212 speed was relatively high, commonly above 1.5 ms<sup>-1</sup>. TMA-, DEA-, and DPA-  
 213 containing particles started accumulating after 01/26/2016 when wind speed was low  
 214 (0.8 ms<sup>-1</sup>) and wind direction from the northwest. After 02/03/2016, DEA- and DPA-  
 215 containing particles showed regular diurnal patterns with high levels of hourly count

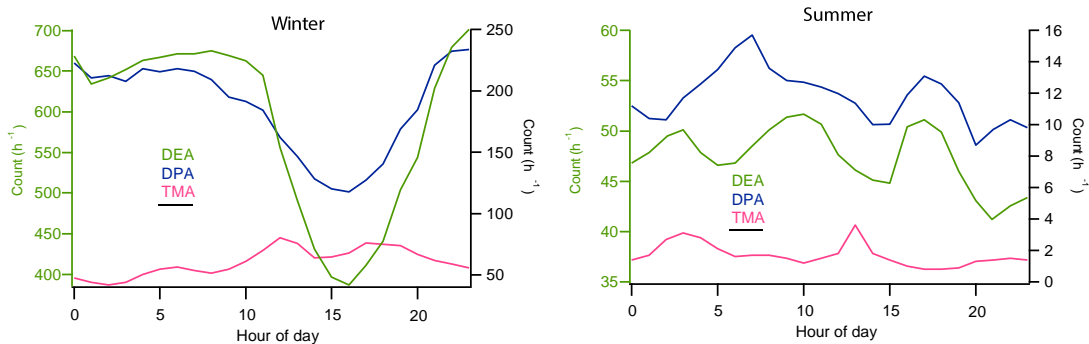
216 during daytime on most days and minimum levels at 15:00. A similar diurnal pattern  
217 was also observed for DPA-containing particles during wintertime (Figures 3a and 3b).  
218 TMA-containing particles presented a complex diurnal profile with peaks in the early  
219 morning (4:00), at noon (12:00) and in the afternoon (18:00). The chemical composition  
220 and diurnal pattern of TMA-containing particles were strongly connected to traffic  
221 emissions.

222 Wind direction and number count of amine-containing particles were analyzed together  
223 using bivariate polar plots (Figure 4). During wintertime, the dominant direction for  
224 amine-containing particles was from the northwest where a forest park was located.  
225 After being emitted from vegetation (plants, grass, and trees) (Ge et al., 2011a), DEA  
226 could partition to the pre-existing particles before arriving at the sampling site. The  
227 transport of these particles to the sampling site caused the elevation in the morning.  
228 Based on the excellent correlation between DEA- and DPA-containing particles, DPA-  
229 containing particles could also be from vegetation. It can be concluded that the major  
230 source of amines in DEA- and DPA-containing particles was vegetation from the  
231 northwest.



232

233 Figure 2. Temporal trends of relative humidity (RH), temperature (Temp.), hourly peak area (dark gray), and particle count (green) of DEA ( $m/z$  74), DPA ( $m/z$  86), and TMA  
 234 ( $m/z$  59) -containing particles in winter (top panel) and summer (bottom panel). The  
 235 black lines in the two panels indicate RH of 90%.  
 236



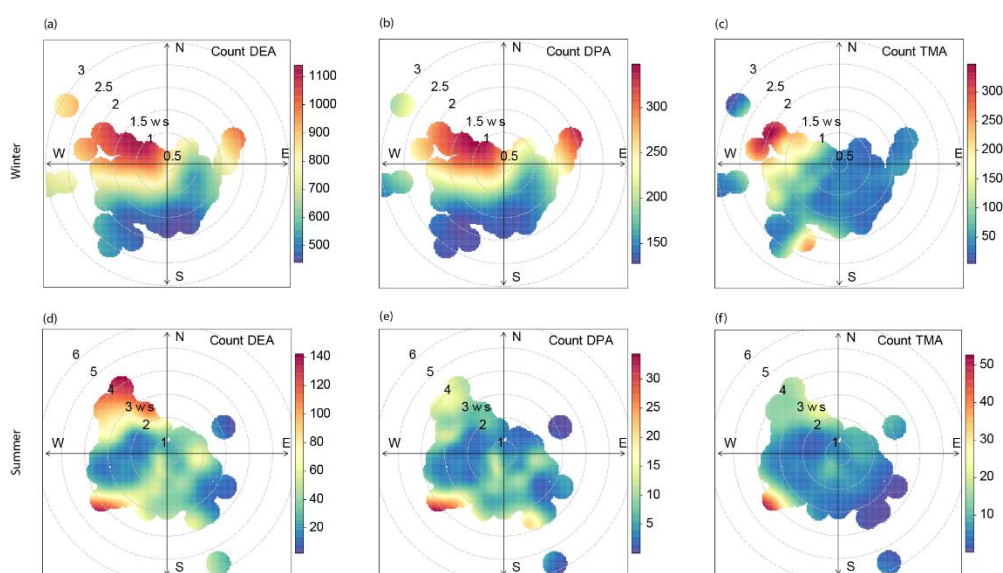
237

238 Figure 3. Diurnal profiles of amine-containing particles during both winter (left panel)  
 239 and summer (right panel). The green left axis in each panel indicates the average  
 240 number count of DEA-containing particles, while the right-axis represents the number  
 241 count of both DPA- and TMA-containing particles.

242 During summer, the amine particles appeared in several episodes; each episode lasted  
 243 for 1~3 days. In these episodes, DPA-containing particles had two rush-hour peaks  
 244 (7:00 and 17:00), likely from traffic (Dall'Osto et al., 2016). Besides traffic, vegetation  
 245 is also a source of DPA-containing particles (from the southwest, Figure 4e). The DPA-  
 246 containing particles peaked 0.84  $\mu\text{m}$ , suggesting that they were not freshly-emitted and  
 247 had undergone substantial aging processes. Moreover, as shown in Figure S2, the mass  
 248 spectra of the amines were present with aromatic hydrocarbon fragments, such as  $\text{C}_4\text{H}_3^+$   
 249 ( $m/z$  51),  $\text{C}_5\text{H}_3^+$  ( $m/z$  63),  $\text{C}_6\text{H}_5^+$  ( $m/z$  77), and  $\text{C}_9\text{H}_8^+$  ( $m/z$  116), as well as with alkanes  
 250 fragments such as  $\text{C}_4\text{H}_7^+$  ( $m/z$  55),  $\text{C}_4\text{H}_9^+$  ( $m/z$  57), and  $\text{C}_5\text{H}_9^+$  ( $m/z$  69). The chemical  
 251 composition of DPA-containing particles contained markers associated with traffic  
 252 emissions. In addition, a similar amine-containing particle type has been reported in the  
 253 literature (Dall'Osto et al., 2016).

254 In summer, DEA-containing particles had a diurnal pattern of three peaks appearing at  
 255 3:00, 9:00 and 17:00. TMA-containing particles had an early morning (4:00) and a noon  
 256 peak (12:00). The morning peaks of DEA- and TMA-containing particles could be due

257 to the local traffic emissions; specifically, heavy-duty vehicles were only allowed to  
258 enter the urban area between 00:00 and 6:00 (Chen et al., 2017). The polar plots showed  
259 that DEA-containing particles were from the northwest and southwest, passing through  
260 the forest park and traffic hub, respectively. This scenario seemed to be inconsistent  
261 with the wintertime results because of the limited traffic contributions to particle levels  
262 in winter. In addition, due to the competition between vegetation and traffic in summer,  
263 the number count and peak area of all three amine-containing particles were poorly  
264 correlated with each other.



265

266 Figure 4. Polar plots of amine-containing particles during winter- and summertime. The  
267 axes in each figure indicate hourly count of each particle type and the colors within the  
268 circles represent wind speed (ws)

### 269 3.3 Effect of RH on the enrichment of DEA-containing particles

270 DEA-containing particles were predominant in both winter and summer, providing a  
271 unique opportunity for investigating DEA processing. Indeed, this kind of discussion  
272 should be treated cautiously and the influences of wind speed, wind direction,

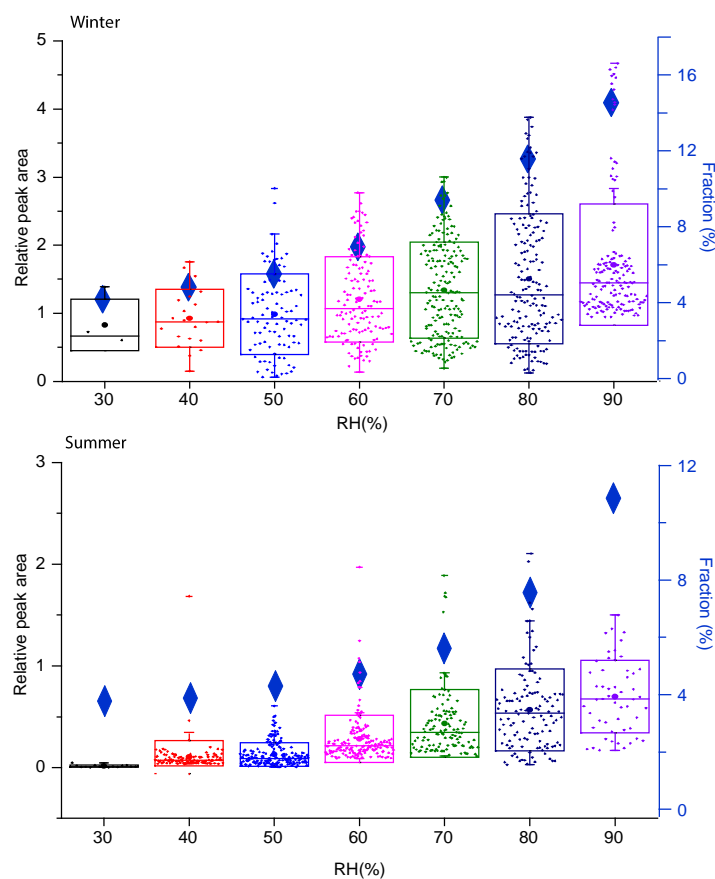
273 temperature, and planetary boundary layer reduction should be removed. As described  
274 above, the average wind speed in both winter and summer was  $1.2 \text{ ms}^{-1}$  and  $1.5 \text{ ms}^{-1}$ ,  
275 respectively. In these stagnant air conditions, the sampled particles were generally local.  
276 Temperature could influence the gas-particle phase partitioning. Assuming the Henry's  
277 Law constants ( $K_H$ ) and the enthalpy change  $\Delta_r H_o(K_H)$  of DEA are constant, a variation  
278 of  $10^\circ\text{C}$  in both summer and winter has negligible influence on the partitioning of  
279 amines from the gas phase to the particle phase, according to the Clapeyron equation  
280 (Ge et al., 2011b). In addition, the shift in planetary boundary layer (PBL) height could  
281 affect the number count and concentration of PM. The relative peak area (RPA) is  
282 defined as the peak area of each  $m/z$  divided by the total dual-ion mass spectral peak  
283 areas of each particle (Healy et al., 2013). Using the temporal trends of RPA, the  
284 influence of PBL height can be removed because it only shows the relative changes  
285 between different species which are all simultaneously influenced by the shift in the  
286 PBL height.

287 Box plots of DEA relative peak area under different RH are shown in Figure 5. In winter,  
288 the median RPA of amine-containing particles increased by two times when RH  
289 increased from 35% to 95%. Meanwhile, the fraction of DEA-containing particles  
290 increased from 4.0% to 16.6%. In summer, the average RPA of DEA increased by three  
291 times (from 0.25 to 0.75) and the fraction of DEA-containing particles ramped from  
292 3.8% to 12.1% when RH increased from 60% to 90%. These results suggest that RH is  
293 important to the enrichment of DEA in the particle phase. When DEA reacts with HCl,  
294  $\text{H}_2\text{SO}_4$ , and  $\text{HNO}_3$ , it tends to form aminium salts, which are soluble in aerosol water.  
295 Along with the influence of aerosol water content, Ge et al. (2011a) also proposed that  
296 strong aerosol acidity could also enhance the partitioning of DEA in the aqueous phase.  
297 In this study, the relative acidity of amine-containing particles ((sulfate

298 +nitrate)/ammonium, (Yao et al., 2011)) was in a range of 20-150, providing favorable  
299 conditions for the dissolution of DEA. Indeed, due to the nature of SPAMS, the amount  
300 of aerosol water content and pH were unavailable, making it difficult for further  
301 analysis. Overall, these results implied that high RH conditions in Chongqing was  
302 favorable for particle uptake of DEA, and the resulting formation of aminium salts  
303 stabilized pre-existing particles; thus, increased their number concentrations.

304 Rehbein et al. (2011) and Zhang et al. (2012) observed direct links between fog  
305 processing and enhancement of TMA-containing particles. High RH conditions were  
306 favorable for TMA entering the particle phase via gas -particle partitioning (Rehbein et  
307 al., 2011; Zhang et al., 2012). Ge et al. (2011b) argued that TMA in the aerosol phase  
308 was in the form of free base, e.g., amine, not aminium salt; TMA could be dissolved in  
309 the aerosol water content; the formation of TMA-HSO<sub>4</sub> salt was possible, but the  
310 formation of TMA-NO<sub>3</sub> and TMA-Cl was impossible due to the competition with  
311 ammonia. Thus, TMA could enter the aerosol phase by gas-aqueous partitioning, or in  
312 the form of TMA-HSO<sub>4</sub> salt. The mechanism of DEA entering the aerosol phase might  
313 be different from TMA. DEA salts were favorable for forming in aerosol phase (Ge et  
314 al., 2011b). Besides, Pankow (2015) proposed that the absorptive uptake of atmospheric  
315 amines could also be possible on organic aerosols. In the context of single particle  
316 mixing state, the amine-containing particles were internally mixed with hygroscopic  
317 species, e.g., sulfate, nitrate, POA species (C<sub>x</sub>H<sub>y</sub><sup>+</sup>, see section 3.4), and SOA species  
318 (oxalate, C<sub>2</sub>H<sub>3</sub>O<sup>+</sup>). Therefore, the mixing state of amine-containing particles was also  
319 favorable for the uptake of amines via different pathways: the aqueous dissolution of  
320 aminium salts and the absorptive uptake on OA.





321

322 Figure 5. Box plots of the hourly relative peak area of DEA under different RH  
 323 conditions in winter (top panel) and summer (bottom panel). The boxes indicate the  
 324 25<sup>th</sup> and 75<sup>th</sup> percentiles; the dots indicate mean value with each data point representing  
 325 a datum of RPA in an hour size bin. Right axis in each panel and the blue diamonds  
 326 show the average number fraction of amine-containing particles among the whole  
 327 [SPAMS](#) dataset.

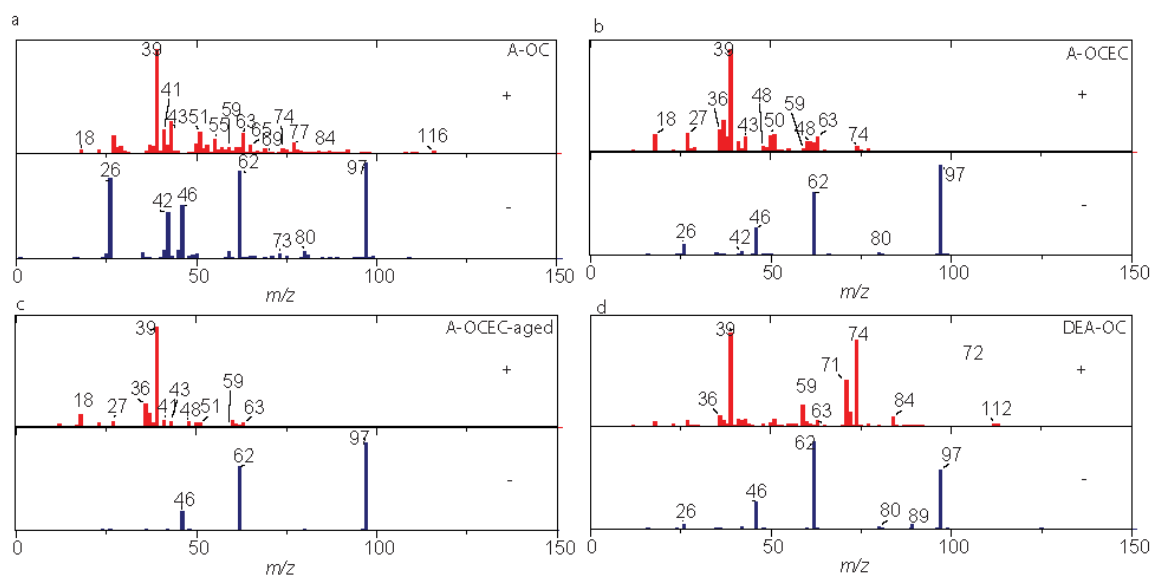
### 328 3.4 Particle types of amine-containing particles

329 As shown in Figure 6, four amine-containing particle types were resolved, including  
 330 amine-OC (A-OC, 41%), A-ECOC (39%), DEA-OC (11%), and A-ECOC-aged (9%).  
 331 All of these particle types had strong signals of amines, and the amines were internally  
 332 mixed with sulfate, nitrate, elemental carbon, and organics.

333 In the A-OC particles, amines were mixed with aromatic hydrocarbon fragments, such  
334 as  $C_4H_3^+$  ( $m/z$  51),  $C_5H_3^+$  ( $m/z$  63),  $C_6H_5^+$  ( $m/z$  77), and  $C_9H_8^+$  ( $m/z$  116), as well as with  
335 alkanes fragments such as  $C_4H_7^+$  ( $m/z$  55),  $C_4H_9^+$  ( $m/z$  57), and  $C_5H_9^+$  ( $m/z$  69). In the  
336 negative mass spectrum of A-OC, strong signals from  $CN^-$  ( $m/z$  -26 ) and  $CNO^-$  ( $m/z$   
337 -42) were typically primary species, along with levoglucosan (Silva et al., 1999). The  
338 amine fragments, such as TMA ( $m/z$  59), DEA ( $m/z$  74), and DPA ( $m/z$  86), were very  
339 abundant in this particle type (76%, 95%, and 88%, respectively). The parent particles  
340 of A-OC were a kind of OC particles from biomass burning; then they mixed with  
341 amines via uptake. Amines could enter the A-OC particle type via dissolution in the  
342 aerosol water content or uptake due to absorptive uptake on the OC aerosol (Pankow,  
343 2015).

344 In A-ECOC mass spectra, strong signals of amines ( $m/z$  59 and 74), along with the  
345 major aromatic hydrocarbon fragments and EC components (i.e.,  $m/z$  36, 48, 60) were  
346 detected. In the negative mass spectra, nitrate and sulfate were also dominant. The A-  
347 ECOC-aged particle type had a similar chemical composition to A-ECOC ( $R^2 = 0.53$ )  
348 but with weaker relative intensities of  $C_xH_y^+$  and amine ions, suggesting it could be  
349 more secondary.

350 In the positive mass spectra of DEA-OC, DEA fragment ( $m/z$  74) was dominant and  
351 present with organic fragments described above. The secondary organic marker ions,  
352 such as  $m/z$  43 ( $[C_2H_3O]^+$ ) and -89 (oxalic acid), were found in the mass spectra.  
353 Besides, DEA-OC was not sensitive to wind speed ( $R^2 = 0.18$ ), implying they were local.



354

355 Figure 6. Average mass spectra of major particle types clustered from amine-containing  
 356 particles.

357 The summertime amine-containing particles were similar to the particle types during  
 358 winter (all  $R^2 > 0.7$ ), except a Ca-rich particle type was also resolved (Figure S5). A-  
 359 Ca-OC particle type was mainly composed of calcium ( $\text{Ca}^+$  and  $\text{CaO}^+$ ), sodium ( $m/z$   
 360 23), potassium ( $m/z$  39), TMA ( $m/z$  59), sulfate, nitrate, and phosphate. An ion signal  
 361 of zinc ( $m/z$  64) was observed in the positive mass spectrum. Zn is a marker for tire  
 362 wear on roads (Grigoratos and Martini, 2015; Thorpe and Harrison, 2008). The A-Ca-  
 363 OC particle type was possibly from traffic activities (Chen et al., 2017).

364 The amine-containing particle types reported in this study were different from those in  
 365 literature. Cheng et al. (2018) reported that  $m/z$  74 amine-containing particles were most  
 366 abundant in the Pearl River Delta, China, but the chemical composition and mixing  
 367 state of amine particles were different from this study. For example, the mixing ratio of  
 368 DPA was much stronger ( $\sim 0.2$ ) in Guangdong than in Chongqing ( $< 0.1$ ). In most related  
 369 studies, TMA-containing particles were dominant, while the present study showed

370 DEA-containing particles were dominant (Rehbein et al., 2011; Zhang et al., 2012;  
371 Healy et al., 2015; Dall'Osto et al., 2016).

#### 372 **4. Conclusions**

373 Amine-containing particles were collected and analyzed during winter and summer in  
374 the urban area of Chongqing. Generally, amine-containing particles were more  
375 abundant in winter than in summer. DEA-containing particles ( $m/z$  74) were the most  
376 important particle type during both summer and winter. Amines were internally mixed  
377 with EC components, organics, sulfate, and nitrate, suggesting particle aging was  
378 significant in both seasons. Amine-containing particles had monomodal size  
379 distributions in the droplet mode, and the distributions peaked at a larger  $D_{va}$  in summer  
380 than winter. DEA- and DPA-containing particles showed strong homogeneity, and  
381 good correlations between the hourly number count and peak area were observed during  
382 winter. The amine-containing particles were mostly from vegetation located southwest  
383 of the sampling area, and traffic sources in the northwest. An enrichment of DEA-  
384 containing particles under high RH conditions was revealed. Reduction of  
385 anthropogenic amines, such as DEA and TMA, would improve the air quality in this  
386 region, which can be achieved by decreasing the emissions of on-road fuel-powered  
387 automobiles.

388 Acknowledgments. Financial support from the National Key Research and  
389 Development Program of China (2018YFC0200403 and 2016YFC0201506), the  
390 Nature Science Foundation of China (Grant No. 41375123), and the Starting-up project  
391 for Ph.D. (15ZA0213) are acknowledged.

392 Author Contribution. CY and YF designed the experiments; TM, SG, PC, WH, and WQ  
393 carried them out; HR, CY, ZL, CJ, and GD analyzed the experiment data; CY prepared  
394 the manuscript with contributions from all co-authors.

## 395 **References**

396 Angelino, S., Suess, D. T., and Prather, K. A.: Formation of aerosol particles from  
397 reactions of secondary and tertiary alkylamines: characterization by aerosol time-of-  
398 flight mass spectrometry, *Environ Sci Technol*, 35, 3130-3138, 10.1021/es0015444,  
399 2001.

400 Bzdek, B. R., Zordan, C. A., Pennington, M. R., Luther, G. W., 3rd, and Johnston, M.  
401 V.: Quantitative assessment of the sulfuric acid contribution to new particle growth,  
402 *Environ Sci Technol*, 46, 4365-4373, 10.1021/es204556c, 2012.

403 Chen, Y., Cao, J., Huang, R., Yang, F., Wang, Q., and Wang, Y.: Characterization,  
404 mixing state, and evolution of urban single particles in Xi'an (China) during wintertime  
405 haze days, *Sci Total Environ*, 573, 937-945, 10.1016/j.scitotenv.2016.08.151, 2016.

406 Chen, Y., Yang, F., Mi, T., Cao, J., Shi, G., Huang, R., Wang, H., Chen, J., Lou, S., and  
407 Wang, Q.: Characterizing the composition and evolution of and urban particles in  
408 Chongqing (China) during summertime, *Atmos Res*, 187, 84-94,  
409 10.1016/j.atmosres.2016.12.005, 2017.

410 Cheng, C. L., Huang, Z. Z., Chan, C. K., Chu, Y. X., Li, M., Zhang, T., Ou, Y. B., Chen,  
411 D. H., Cheng, P., Li, L., Gao, W., Huang, Z. X., Huang, B., Fu, Z., and Zhou, Z.:  
412 Characteristics and mixing state of amine-containing particles at a rural site in the Pearl  
413 River Delta, China, *Atmos Chem Phys*, 18, 9147-9159, 10.5194/acp-18-9147-2018,  
414 2018.

415 Dall'Osto, M., Beddows, D. C. S., McGillicuddy, E. J., Esser-Gietl, J. K., Harrison, R.  
416 M., and Wenger, J. C.: On the simultaneous deployment of two single-particle mass  
417 spectrometers at an urban background and a roadside site during SAPUSS, *Atmos*  
418 *Chem Phys*, 16, 9693-9710, 10.5194/acp-16-9693-2016, 2016.

419 Dallosto, M., and Harrison, R.: Chemical characterisation of single airborne particles  
420 in Athens (Greece) by ATOFMS, *Atmos Environ*, 40, 7614-7631,  
421 10.1016/j.atmosenv.2006.06.053, 2006.

422 De Haan, D. O., Hawkins, L. N., Kononenko, J. A., Turley, J. J., Corrigan, A. L.,  
423 Tolbert, M. A., and Jimenez, J. L.: Formation of nitrogen-containing oligomers by  
424 methylglyoxal and amines in simulated evaporating cloud droplets, *Environ Sci*  
425 *Technol*, 45, 984-991, 10.1021/es102933x, 2011.

426 Denkenberger, K. A., Moffet, R. C., Holecek, J. C., Rebotier, T. P., and Prather, K. A.:  
427 Real-time, single-particle measurements of oligomers in aged ambient aerosol particles,  
428 *Environ Sci Technol*, 41, 5439-5446, 10.1021/es0703291, 2007.

429 Ge, X., Wexler, A. S., and Clegg, S. L.: Atmospheric amines – Part I. A review, *Atmos*  
430 *Environ*, 45, 524-546, 10.1016/j.atmosenv.2010.10.012, 2011a.

431 Ge, X., Wexler, A. S., and Clegg, S. L.: Atmospheric amines – Part II. Thermodynamic  
432 properties and gas/particle partitioning, *Atmos Environ*, 45, 561-577,  
433 10.1016/j.atmosenv.2010.10.013, 2011b.

434 Gómez Alvarez, E., Viidanoja, J., Muñoz, A., Wirtz, K., and Hjorth, J.: Experimental  
435 Confirmation of the Dicarbonyl Route in the Photo-oxidation of Toluene and Benzene,  
436 *Environ Sci Technol*, 41, 8362-8369, 10.1021/es0713274, 2007.

437 Grigoratos, T., and Martini, G.: Brake wear particle emissions: a review, *Environ Sci*  
438 *Pollut Res Int*, 22, 2491-2504, 10.1007/s11356-014-3696-8, 2015.

439 Healy, R. M., Sciare, J., Poulain, L., Crippa, M., Wiedensohler, A., Prevot, A. S. H.,  
440 Baltensperger, U., Sarda-Estevé, R., McGuire, M. L., Jeong, C. H., McGillicuddy, E.,  
441 O'Connor, I. P., Sodeau, J. R., Evans, G. J., and Wenger, J. C.: Quantitative  
442 determination of carbonaceous particle mixing state in Paris using single-particle mass  
443 spectrometer and aerosol mass spectrometer measurements, *Atmos Chem Phys*, 13,  
444 9479-9496, 10.5194/acp-13-9479-2013, 2013.

445 Healy, R. M., Evans, G. J., Murphy, M., Sierau, B., Arndt, J., McGillicuddy, E.,  
446 O'Connor, I. P., Sodeau, J. R., and Wenger, J. C.: Single-particle speciation of  
447 alkylamines in ambient aerosol at five European sites, *Anal Bioanal Chem*, 407, 5899-  
448 5909, 10.1007/s00216-014-8092-1, 2015.

449 Huang, Q., Cai, X., Song, Y., and Zhu, T.: Air stagnation in China (1985–2014):  
450 climatological mean features and trends, *Atmos. Chem. Phys.*, 17, 7793-7805,  
451 10.5194/acp-17-7793-2017, 2017.

452 Huang, Y., Chen, H., Wang, L., Yang, X., and Chen, J.: Single particle analysis of  
453 amines in ambient aerosol in Shanghai, *Environ Chem*, 9, 202-210, 10.1071/en11145,  
454 2012.

455 Kirkby, J., Curtius, J., Almeida, J., Dunne, E., Duplissy, J., Ehrhart, S., Franchin, A.,  
456 Gagne, S., Ickes, L., Kurten, A., Kupc, A., Metzger, A., Riccobono, F., Rondo, L.,  
457 Schobesberger, S., Tsagkogeorgas, G., Wimmer, D., Amorim, A., Bianchi, F.,  
458 Breitenlechner, M., David, A., Dommen, J., Downard, A., Ehn, M., Flagan, R. C.,  
459 Haider, S., Hansel, A., Hauser, D., Jud, W., Junninen, H., Kreissl, F., Kvashin, A.,  
460 Laaksonen, A., Lehtipalo, K., Lima, J., Lovejoy, E. R., Makhmutov, V., Mathot, S.,

461 Mikkila, J., Minginette, P., Mogo, S., Nieminen, T., Onnela, A., Pereira, P., Petaja, T.,  
462 Schnitzhofer, R., Seinfeld, J. H., Sipila, M., Stozhkov, Y., Stratmann, F., Tome, A.,  
463 Vanhanen, J., Viisanen, Y., Vrtala, A., Wagner, P. E., Walther, H., Weingartner, E.,  
464 Wex, H., Winkler, P. M., Carslaw, K. S., Worsnop, D. R., Baltensperger, U., and  
465 Kulmala, M.: Role of sulphuric acid, ammonia and galactic cosmic rays in atmospheric  
466 aerosol nucleation, *Nature*, 476, 429-433, 10.1038/nature10343, 2011.

467 Li, L., Huang, Z., Dong, J., Li, M., Gao, W., Nian, H., Fu, Z., Zhang, G., Bi, X., Cheng,  
468 P., and Zhou, Z.: Real time bipolar time-of-flight mass spectrometer for analyzing  
469 single aerosol particles, *Int J Mass Spectrom*, 303, 118-124,  
470 10.1016/j.ijms.2011.01.017, 2011.

471 Li, Y. J., Sun, Y., Zhang, Q., Li, X., Li, M., Zhou, Z., and Chan, C. K.: Real-time  
472 chemical characterization of atmospheric particulate matter in China: A review, *Atmos*  
473 *Environ*, 2017.

474 Moffet, R. C., de Foy, B., Molina, L. T., Molina, M. J., and Prather, K. A.: Measurement  
475 of ambient aerosols in northern Mexico City by single particle mass spectrometry,  
476 *Atmos. Chem. Phys.*, 8, 4499-4516, 10.5194/acp-8-4499-2008, 2008.

477 Monks, P. S.: Gas-phase radical chemistry in the troposphere, *Chem Soc Rev*, 34, 376-  
478 395, 10.1039/b307982c, 2005.

479 Onasch, T. B., Trimborn, a., Fortner, E. C., Jayne, J. T., Kok, G. L., Williams, L. R.,  
480 Davidovits, P., and Worsnop, D. R.: Soot Particle Aerosol Mass Spectrometer:  
481 Development, Validation, and Initial Application, *Aerosol Sci. Technol.*, 46, 804-817,  
482 10.1080/02786826.2012.663948, 2012.



483 Pankow, J. F.: Phase considerations in the gas/particle partitioning of organic amines  
484 in the atmosphere, *Atmos Environ*, 122, 448-453, 10.1016/j.atmosenv.2015.09.056,  
485 2015.

486 Pratt, K. A., Murphy, S. M., Subramanian, R., DeMott, P. J., Kok, G. L., Campos, T.,  
487 Rogers, D. C., Prenni, A. J., Heymsfield, A. J., Seinfeld, J. H., and Prather, K. A.:  
488 Flight-based chemical characterization of biomass burning aerosols within two  
489 prescribed burn smoke plumes, *Atmos Chem Phys*, 11, 12549-12565, 10.5194/acp-11-  
490 12549-2011, 2011.

491 Qin, X., Pratt, K. A., Shields, L. G., Toner, S. M., and Prather, K. A.: Seasonal  
492 comparisons of single-particle chemical mixing state in Riverside, CA, *Atmos Environ*,  
493 59, 587-596, 10.1016/j.atmosenv.2012.05.032, 2012.

494 Rehbein, P. J., Jeong, C. H., McGuire, M. L., Yao, X., Corbin, J. C., and Evans, G. J.:  
495 Cloud and fog processing enhanced gas-to-particle partitioning of trimethylamine,  
496 *Environ Sci Technol*, 45, 4346-4352, 10.1021/es1042113, 2011.

497 Silva, P. J., Liu, D.-Y., Noble, C. A., and Prather, K. A.: Size and Chemical  
498 Characterization of Individual Particles Resulting from Biomass Burning of Local  
499 Southern California Species, *Environ Sci Technol*, 33, 3068-3076, 10.1021/es980544p,  
500 1999.

501 Smith, J. N., Barsanti, K. C., Friedli, H. R., Ehn, M., Kulmala, M., Collins, D. R.,  
502 Scheckman, J. H., Williams, B. J., and McMurry, P. H.: Observations of aminium salts  
503 in atmospheric nanoparticles and possible climatic implications, *Proc Natl Acad Sci U*  
504 *S A*, 107, 6634-6639, 10.1073/pnas.0912127107, 2010.

505 Song, X. H., Hopke, P. K., Ferguson, D. P., and Prather, K. A.: Classification of single  
506 particles analyzed by ATOFMS using an artificial neural network, ART-2A, Anal.  
507 Chem., 71, 860-865, DOI 10.1021/ac9809682, 1999.

508 Tan, P. V., Evans, G. J., Tsai, J., Owega, S., Fila, M. S., Malpica, O., and Brook, J. R.:  
509 On-line analysis of urban particulate matter focusing on elevated wintertime aerosol  
510 concentrations, Environ Sci Technol, 36, 3512-3518, 10.1021/es011448i, 2002.

511 Tao, J., Zhang, L., Cao, J., and Zhang, R.: A review of current knowledge concerning  
512 PM<sub>2.5</sub>; chemical composition, aerosol optical properties and  
513 their relationships across China, Atmos Chem Phys, 17, 9485-9518, 10.5194/acp-17-  
514 9485-2017, 2017.

515 Thorpe, A., and Harrison, R. M.: Sources and properties of non-exhaust particulate  
516 matter from road traffic: a review, Sci Total Environ, 400, 270-282,  
517 10.1016/j.scitotenv.2008.06.007, 2008.

518 Wang, J. F., Ge, X. L., Chen, Y. F., Shen, Y. F., Zhang, Q., Sun, Y. L., Xu, J. Z., Ge,  
519 S., Yu, H., and Chen, M. D.: Highly time-resolved urban aerosol characteristics during  
520 springtime in Yangtze River Delta, China: insights from soot particle aerosol mass  
521 spectrometry, Atmos Chem Phys, 16, 9109-9127, 10.5194/acp-16-9109-2016, 2016.

522 Wang, L., Khalizov, A. F., Zheng, J., Xu, W., Ma, Y., Lal, V., and Zhang, R.:  
523 Atmospheric nanoparticles formed from heterogeneous reactions of organics, Nature  
524 Geoscience, 3, 238, 10.1038/ngeo778  
525 <https://www.nature.com/articles/ngeo778#supplementary-information>, 2010.

526 Yao, L., Garmash, O., Bianchi, F., Zheng, J., Yan, C., Kontkanen, J., Junninen, H.,  
527 Mazon, S. B., Ehn, M., Paasonen, P., Sipila, M., Wang, M., Wang, X., Xiao, S., Chen,

528 H., Lu, Y., Zhang, B., Wang, D., Fu, Q., Geng, F., Li, L., Wang, H., Qiao, L., Yang,  
529 X., Chen, J., Kerminen, V. M., Petaja, T., Worsnop, D. R., Kulmala, M., and Wang, L.:  
530 Atmospheric new particle formation from sulfuric acid and amines in a Chinese  
531 megacity, *Science*, 361, 278-281, 10.1126/science.aao4839, 2018.

532 Yao, X., Rehbein, P. J. G., Lee, C. J., Evans, G. J., Corbin, J., and Jeong, C.-H.: A study  
533 on the extent of neutralization of sulphate aerosol through laboratory and field  
534 experiments using an ATOFMS and a GPIC, *Atmos Environ*, 45, 6251-6256,  
535 10.1016/j.atmosenv.2011.06.061, 2011.

536 You, Y., Kanawade, V. P., de Gouw, J. A., Guenther, A. B., Madronich, S., Sierra-  
537 Hernández, M. R., Lawler, M., Smith, J. N., Takahama, S., Ruggeri, G., Koss, A., Olson,  
538 K., Baumann, K., Weber, R. J., Nenes, A., Guo, H., Edgerton, E. S., Porcelli, L., Brune,  
539 W. H., Goldstein, A. H., and Lee, S. H.: Atmospheric amines and ammonia measured  
540 with a chemical ionization mass spectrometer (CIMS), *Atmos. Chem. Phys.*, 14, 12181-  
541 12194, 10.5194/acp-14-12181-2014, 2014.

542 Zhang, G., Bi, X., Chan, L. Y., Li, L., Wang, X., Feng, J., Sheng, G., Fu, J., Li, M., and  
543 Zhou, Z.: Enhanced trimethylamine-containing particles during fog events detected by  
544 single particle aerosol mass spectrometry in urban Guangzhou, China, *Atmos Environ*,  
545 55, 121-126, 10.1016/j.atmosenv.2012.03.038, 2012.

546